# RSC Advances

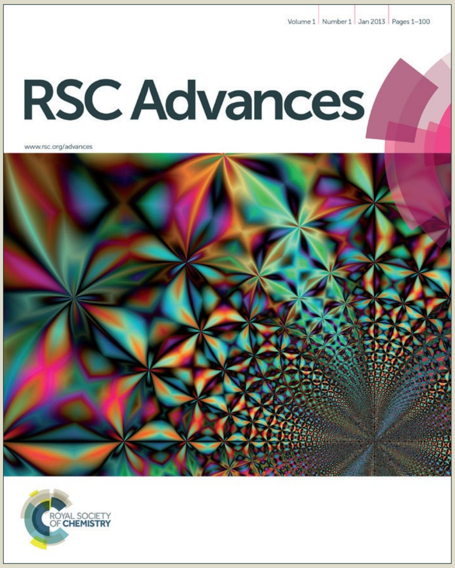




ROYAL SOCIETY OF CHEMISTRY

www.rsc.org/advances

# A Three-Dimensional $MnO_2$/Graphene hybrid as binder-free supercapacitor electrode

Chuanyin Xiong*, Tiehu Li*, Muhammad Khan, Hao Li, Tingkai Zhao

School of Materials Science and Engineering, Northwestern Polytechnical University, Xi'an 710072, PR China



* Corresponding author. Tel.:+86 029 88460337; fax: +86 029 88460337.

E-mail address: xiongchuanyin@126.com

**Abstract:** Highly aligned manganese dioxide ($MnO_2$) nanowall arrays electrodeposited onto Ti sheets are used as substrates to grow graphene (GR) through chemical vapor deposition (CVD), thus forming three-dimensional (3D) $MnO_2$/GR hybrid composite. Furthermore, 3D $MnO_2$/GR hybrid with different structures and properties has been prepared at different temperatures. The as-prepared hybrid materials could be directly used as supercapacitor electrodes without any binder and conductive additive, and fully maintain the high conductivity and high specific area of GR, large pseudocapacitance of $MnO_2$ nanowall arrays. In aqueous electrolytes, the hybrids show a high specific capacitance of ~326.33 F $g^{-1}$ with good cycling stability at the scan rate of 200 mV $s^{-1}$ and high energy density of 23.68 Wh $kg^{-1}$ while maintaining high power density of 7270 W $kg^{-1}$. The preparation method provides a novel road to fabricate 3D graphene-based composite materials, and the so obtained hybrid electrode demonstrates its potential applications in supercapacitors.

**Keywords:** Manganese dioxide nanowall arrays, Electrodeposited, Graphene, Three-dimensional, Energy density, Supercapacitor

## 1. Introduction

In response to the gradual depletion of fossil fuels and the increasing severity of environmental pollution problems, developing sustainable and renewable energy storage devices has become increasingly urgent in order to meet the future demands. Supercapacitors are regarded as an efficient and environmental friendly energy storage and supply technology for its high power density and low pollution. Such "high power-density" devices, however, has low energy density compared to batteries. To improve the performance and promote the commercialization of supercapacitors, it is important to explore new electrode materials with low cost, high performance and environmental benignity. Carbon-based materials, as supercapacitor electrodes are widely concerned [1-7] due to their low cost and good electrical conductivity. Thereinto graphene (GR) is the ideal electrode materials because of the outstanding electrical conductivity, large specific surface area and mechanical properties. So far many methods have been developed to prepare graphene [8-12] including chemical vapor deposition (CVD) [8], micromechanical cleavage [9,10], and chemical reduction of graphite oxide (GO) [11,12]. Among these methods, chemical reduction of GO is the predominant method in the mass production of graphene for industrial applications. However, GR exhibits an undesired specific surface area (200-500 $m^2$ $g^{-1}$) far below its theoretical value (2675 $m^2$ $g^{-1}$) due to the intensive stacking among these two dimensional sheets. To solve this problem, 3D GR has become a hot research topic [13,14] because this structure could sufficiently maintain the features of individual GR and generate a large specific surface area. Shi *et al*. reported a 3D mechanically strong, electrically conductive, and thermally stable self-assembled GR hydrogel (SGH) with a high specific capacitance, which was prepared from GO by a one-step hydrothermal method [13], however, the as-prepared composite suffered from poor conductivity with the presence of a large amount of water. Bong *et al*. fabricated assembled embossed chemically modified GR film by using polystyrene colloidal particles as a sacrificial template and explored its use in supercapacitor electrodes [14]. Nevertheless, this three-dimensional GR structure is unstable and easy to collapse.

Currently, metal oxides have been extensively applied as the spacer to separate GR nanosheets in view of their high pseudocapacitance [15-17]. Among metal oxides, manganese dioxide ($MnO_2$) is regarded as a promising candidate for supercapacitors due to its low cost, high natural abundance, high theoretical capacity(~1370 F $g^{-1}$), and non-toxicity [18,19]. More significantly, unlike other electrode materials, which should be used in strong acidic or alkaline electrolytes, $MnO_2$ can be used in neutral aqueous electrolytes, and hence can meet the requirements for "green electrolyte" in supercapacitors. Futhermore, compared to some traditional backing materials such as Ni、Co、Pt、Ru *et al.* [20], $MnO_2$ used as a substrate to grow GR is beneficial to reduce CVD reaction temperature, however, the low surface area and poor electronic conductivity ($10^{-5}$-$10^{-6}$S $cm^{-1}$) remain the major problems. One promising approach is to fabricate 3D $MnO_2$/GR composite structures, where the hybrid can obtain the synergistic effect of individual constituents. Various approaches to synthesize 3D $MnO_2$/GR electrodes have been reported [15-17], including physical mixing, microwave-assisted method, chemical co-precipitation and electrochemical deposition. For instance, $MnO_2$/GR electrodes synthesized by soft chemical route exhibited a specific capacitance (SC) of 210 F $g^{-1}$ [15] and those produced by microwave-assisted method displayed SC of 310 F $g^{-1}$ [16]. Cheng *et al.* reported a maximum energy density of 30.4 Wh $kg^{-1}$ and power density of 5 kW $kg^{-1}$ using GR//$MnO_2$/GR hybrid cells [17].

In this work, an effective two-step approach is developed to fabricate high-quality but low cost 3D $MnO_2$/GR hybrids through one-step CVD and an electrodeposition method. The so-obtained 3D $MnO_2$/GR hybrid presents a high specific capacitance of 326.33 F $g^{-1}$ at the scan rates of 200 mV $s^{-1}$ with capacitance retention of ~92% and a high energy density of 23.68 Wh $kg^{-1}$ after 1000 cyclic voltammogram (CV) cycles.

## 2. Experimental

2.1 Preparation of substrate of aligned $MnO_2$ nanowall arrays

The precursor solutions were prepared by dissolving manganese acetate, $Mn(CH_3COO)_2 \cdot 4H_2O$ (99+%, Alfa Aesar) and anhydrous sodium sulfate, $Na_2SO_4$ (99%, J. T. Baker) into deionised (DI) water in a concentration of 0.15 M for both precursors. The solution was stirred at room temperature for 1 h to ensure the complete dissolution of both solutes prior to the electrodeposition experiments.

Schematic illustration of electrodeposition of the $MnO_2$ nanowall arrays was presented in Figure S1. Highly aligned $MnO_2$ nanowall arrays were obtained by cathodic electrodeposition onto a Ti substrate with an exposed surface area of 1 $cm^2$. Ti sheets were rinsed with ethanol and acetone before electrochemical deposition. The anode and cathode of the adjustable constant voltage source is connected to two same Ti sheets, separately (The horizontal distance between the two sheets is 2 cm). The Ti sheets were soak in a mixed aqueous solution of manganese acetate and sodium sulfate. The deposition was induced by a change of the voltage (voltage was maintained between 5.0 - 8.0 V). The deposition time was controlled within 15 mins.

2.2 Fabrication of $MnO_2$/GR composites

The preparation process was shown in Scheme 1. The aligned $MnO_2$ nanowall arrays on the surface of Ti substrate were placed into the tube furnace and heated to 600, 700 $^{o}$C, individually at the heating rate of 15 $^{o}$C min$^{-1}$ under Ar (200 s.c.c.m.) and $H_2$ (100 s.c.c.m.). 0.25 mL of benzene used as carbon source was injected into the furnace at the rate of 0.01 mL min$^{-1}$ for 30 mins. After 5 min of reaction-gas mixture flow, the samples were rapidly cooled to room temperature at a rate of 100 $^{o}$C min$^{-1}$ under Ar (200 s.c.c.m.) and $H_2$ (100 s.c.c.m.). A series of 3D $MnO_2$/GR composites were prepared and denoted as $MnO_2$/GR600, $MnO_2$/GR700, $MnO_2$/GR800, respectively.

2.3. Material characterization

The morphologies and microstructures of the samples were examined by scanning electron microscopy (SEM; XL30), transmission electron microscopy (TEM; Hitachi H-600), and High Resolution TEM (HRTEM). The crystal structures of the as-prepared products were characterized by an X-ray diffractometer (XRD; D/Max 2500 V PC$^{-1}$, Cu-Ka radiation) with a scan speed of 2 min$^{-1}$. Raman spectra were collected through a Renishaw 2000 model confocal microscopy Raman spectrometer with a CCD detector and a holographic notch filter (Renishaw Ltd., Gloucestershire, U.K.) at ambient conditions, using the radiation of 514.5 nm from an air-cooled argon ion laser to excite the SERS.

2.4. Electrochemical measurements

The electrochemical experiments were carried out using a two-electrode system at ambient temperature, with 1.5 M $Li_2SO_4$ as the electrolyte solution. The as-synthesized materials were directly used as the working electrode and the counter electrode, respectively. Electrochemical measurements were all conducted on a CHI 660D electrochemical workstation (Shanghai, Chenhua). The CV curves of the electrodes were measured between 0 and 1.2 V at different scan rates from 50 to 400 mV $s^{-1}$. The galvano-static cycling for each electrode was performed in the potential range from 0 to 1 V at different current densities of 1, 1.5, 2, 2.5 and 3 A $g^{-1}$, and electrochemical impedance spectroscopy (EIS) measurements were carried out in the frequency range of 100 kHz ~ 1 Hz.

## 3. Results and discussion

### 3.1. Structure and morphology

Fig. 1A presents the photographs of Ti, $MnO_2$, $MnO_2$700 ($MnO_2$ heated in 700 $^oC$) and $MnO_2$/GR composites at different temperatures. It can be seen that the white original Ti plate changes to yellow after electrodeposition of $MnO_2$. After GR grown on the surface of $MnO_2$ through CVD, the color of the materials changes gradually into black, which indicates that the surface of $MnO_2$ is coated with a layer of carbon. In order to investigate whether the morphology of $MnO_2$ is destroyed at high temperature, a comparison of the pristine $MnO_2$ and heated $MnO_2$ is necessary. Fig. 1B,C show two SEM images of $MnO_2$ before and after the heating process (700 ℃). Clearly, electrodeposition synthesis of the flower-like $MnO_2$ nanostructures can be observed before and after the heating process, which demonstrates that the morphology of $MnO_2$ is not destroyed after the heating process. More significantly, the flower-like $MnO_2$ nanostructures can provide the high accessibility of electrolytic ions for shorten diffusion paths, which is beneficial to obtain good electrochemical capacitance performance. Unfortunately, when the $MnO_2$ sample is heated to 800 ℃ (Figure S2), the flower-like $MnO_2$ nanostructures has been destroyed. Fig. 1D,E show the SEM images of GR grown on the surfaces of $MnO_2$ nanowall substrates at different temperatures (600 and 700 °C), respectively. The surfaces of $MnO_2$ nanowall substrates are both covered with a layer of GR, which will be further confirmed in the Raman test.

The XRD patterns of the GR grown on the surface of the $MnO_2$ nanowall substrates at 600 and 700 °C are shown in Fig. 2A. Two characteristic peaks of the $MnO_2$ at $2\theta$ around 37° and 66° are displayed, which can be indexed to birnessite-type $MnO_2$ (JCPDS 42-1317) [21]. Furthermore, from the XRD analysis, the d-spacing of $MnO_2$ is about 7.0 Å, which is consistent with the high magnification TEM image (Fig. 3B) and the previous report [22]. The diffraction peaks at 2θ around 43° that is in keeping with the literature report [23] indicates that GR has been obtained successfully on the surface of the $MnO_2$ nanowall arrys after CVD.

The structure of 3D $MnO_2$/GR composites are further confirmed by Raman spectra (Fig. 2B). Except from the D band (about1350 $cm^{-1}$) and G band (1590 $cm^{-1}$) associated with GR, the major Raman bands located at 500-700 $cm^{-1}$ for $MnO_2$/GR sample matches well with the major vibrational features of $MnO_2$ compounds reported previously [22]. Furthermore, compared to the value of $I_D/I_G$ at 600 °C, the lower value at 700 °C indicates fewer defects. Consequently, the following tests are based on $MnO_2$/GR700.

The microstructure of the $MnO_2$/GR700 composite is further investigated by TEM (see Fig. 3). Obviously, the GR sheets are closely attached on the surface of the $MnO_2$ nanowall arrays (Fig. 3A). The flower-like morphology is the characteristic of the birnessite-type $MnO_2$ [24,25]. As shown in Fig. 3B, the interplanar spacing of $MnO_2$ nanowall arrays and the GR sheets are measured to be 0.7 and 0.34 nm, respectively, which are in line with the literature report for birnessite-type $MnO_2$ [24]. To investigate the morphology of GR, the TEM image of GR is examined by etching away $MnO_2$ with 3 M HCl. The ultrathin morphology of the derived GR can be seen clearly in Fig. 3C. The related EDS spectrum (Fig. 3D) reveals the Mn, O signal from $MnO_2$ as expected. The C signal is derived from the GR and the Ti signal is derived from the Ti sheets.

3.2. Electrochemical properties

To evaluate the electrical behaviour of the as-fabricated 3D $MnO_2$/GR700 hybrids, the electrochemical capacitive performance for each type of electrode is measured by CV, galvanostatic charge-discharge (GCD) and EIS tests. The CV profiles of electrodeposition of $MnO_2$700 nanowall arrays (Figure S3) at different scan rates from 50 to 400 mV $s^{-1}$ show nearly rectangular shapes, indicating good pseudocapacitive behavior attributed to a continuous and reversible Faradaic redox transition of $MnO_2$ over the potential range. Furthermore, Fig. 4A shows the CV curves of the $MnO_2$/GR700 hybrid at various scan rates ranging from 50 to 400 mV $s^{-1}$ within an electrochemical window from 0 to 1.2 V. As the scan rate increases, the current response also increases without any obvious change in the shape of the CV curves, which presents a good rate performance. The rectangular and symmetric shape of the CV curve is also observed at a high scan rate of 400 mV $s^{-1}$ due to the low contact resistance of the electrode. Fig. 4B displays a comparision of CV curves of $MnO_2$, $MnO_2$/GR600, $MnO_2$/GR700 and $MnO_2$/GR800 hybrids at a scan rate of 200 mV $s^{-1}$. The specific capacitance can be calculated according to the following equation: [26,27]

$$C_m = \int_{V_1}^{V_2} |I| dV \Big/ 2mv\Delta V$$

where $C_m$ is the specific capacitance (F $g^{-1}$), I is the response current (A), m (~0.1 mg) is the mass of the electroactive materials (g), and $\Delta V$ is the potential window during the CV measurements process (V). The specific capacitances of $MnO_2$, $MnO_2$/GR600, $MnO_2$/GR700 and $MnO_2$/GR800 electrodes are 183.23 F $g^{-1}$, 208.76 F $g^{-1}$, 326.33 F $g^{-1}$ and 136.28 F $g^{-1}$, respectively. Hence, we can confirm that the GR supplies a large double layer capacitance while $MnO_2$ provides a large pseudocapacitive contribution to the capacitance of $MnO_2$/GR. In addition, more than 60% decrease in the capacitance of $MnO_2$/GR800 supports the SEM analysis of $MnO_2$/GR800 hybrid (Figure S2). Therefore, the optimal temperature for the growth of GR on $MnO_2$ substrates should be 700 ℃. Furthermore, the picture in Fig. 4C is the CV curve of $MnO_2$ at the scan rate of 100 mV $s^{-1}$. It presents a bigger voltage drop compared with the $MnO_2$/GR hybrid, which implies that the internal resistance has decreased largely after the growth of GR on the surface of the $MnO_2$ nanowall arrays. This is because GR in the hybrid acts as electronic conductive channels to increase the electrical conductivity, which matches well with the GCD curves of the $MnO_2$/GR (Fig. 4D). Fig. 4D shows GCD curves for $MnO_2$, $MnO_2$/GR700 electrodes at the current density of 3.0 A $g^{-1}$. It can be seen that the curve are highly linear and symmetrical without obvious voltage drop compared with the $MnO_2$, indicating a rapid I-V response, an excellent electrochemical reversibility and little overall resistance of this material (more data about the GCD curves of $MnO_2$/GR700 electrode at different current densities of 1, 1.5, 2, 2.5 and 3 A

$g^{-1}$ are given in Figure S4 in the support information). It can be seen from Figure S4 that all the GCD curves of $MnO_2$/GR700 at different current densities are highly linear and almost typical isosceles triangular in shape, which further demonstrates that the electrode has ideal capacitive characteristics and excellent electrochemical reversibility. EIS measurements are carried out in a frequency range of 100 kHz to 1 Hz to further evaluate the electrochemical and structural characteristics of the electrode material (Fig. 4E). Compared with the $MnO_2$, the EIS Nyquist plot of the $MnO_2$/GR700 has a shorter arc located at high frequencies followed by an inclined line with a slope about 45°. The span of the arc is indicative of the charge-transfer resistances of the electrode materials [28]. It can make clear from Fig. 4E that, the span of the arc in Nyquist plot decreases when GR is added, which is consistent with the results of the CV and GCD studies. Obviously, the low resistances of $MnO_2$/GR700 electrode should stem from their intrinsic high conductivity, rich porous 3D network and the flower-like morphology of $MnO_2$. Fig. 4F displays the cyclic stability of $MnO_2$/GR700 at the scan rate of 200 mV $s^{-1}$ for 1000 cycles. It is clear that the $MnO_2$/GR700 electrode presents long-term cycle stability with capacitance retention of ~92% after 1000 CV cycles (approximately 300 F $g^{-1}$). These results fully reflect the merit of the 3D architecture cherished by the $MnO_2$/GR electrode.

Energy and power densities are two crucial parameters for evaluating the electrochemical performance of supercapacitors. The energy density ( E in Wh $kg^{-1}$ ) and power density ( P in W $kg^{-1}$ ) of the electrode can be further evaluated from the CV curves at different scan rates using the following equations (1) and (2), respectively:

[29]

$$E = {C_m \Delta V^2}/{2} \quad (1)$$

$$P = {E}/{t} \quad (2)$$

where $C_m$ is the specific capacitance (F $g^{-1}$), $\Delta V$ is the potential window during the CV measurements process (V) and t is the discharge time of the CV curves (s). Fig. 5 exhibits the energy and power density for the $MnO_2$/GR700 hybrid electrode, where the reported data of some typical energy storage device such as batteries [30] and $MnO_2$-carbon based supercapacitors [18,31-36]. By comparison, our work displays a high energy density of 23.68 Wh $kg^{-1}$ while maintaining high power density of 7270 W $kg^{-1}$ at the scan rate of 200 mV $s^{-1}$, which can be comparable with the previously reported high-performance energy-storage devices (the related data are displayed in the Table S1 in the support information). In addition, more data for large mass loading (1 and 3 mg) are also given in Figure S5 (A, B) in the support information. Obviously, the results are consistent with the analysis results of Fig. 4A, and the energy and power densities can reach to 24.86, 25.13 Wh $kg^{-1}$ and 6997, 6812 W $kg^{-1}$ at scan rate of 200 mV $s^{-1}$, respectively, which also displays high-performance electrochemical energy-storage of 3D $MnO_2$/GR700 electrode. Thus, it is to be expected: the as-fabricated 3D $MnO_2$/GR hybrid has enormous potential applications in supercapacitors.

## 4.Conclusions

In summary, a novel strategy has been put forward to fabricate 3D $MnO_2$/GR hybrid through chemical vapor deposition on the substrate of aligned $MnO_2$ nanowall arrays that were electrochemically deposited onto Ti sheets. An optimal condition of preparation has been also obtained by comparing the electrical behaviour of $MnO_2$/GR hybrid electrodes fabricated at different temperatures. The as-synthesized $MnO_2$/GR700 electrode shows a specific capacitance of 326.33 F $g^{-1}$ at the scan rate of 200 mV $s^{-1}$ and can be cycled reversibly in the voltage region of 0 to 1.2 V. Moreover, it can maintain an energy density of 23.68 Wh $kg^{-1}$ even at the power density of 7270 W $kg^{-1}$, which indicates the high-efficiency energy storage of $MnO_2$/GR700 hybrid. We expect this work will open up new opportunities for the application of low-cost, high-efficiency 3D GR-based electrodes materials in new energy electric vehicle.

**Acknowledgments**

This work was supported by the Specialized Research Fund for the Doctoral Program of Higher Education (20116102110014), National Natural Science Foundation of China(Grant No.: 51172184), the Key Science and Technology Program of Shaanxi Province, China (2013K09-03), and the Innovation Fund of China Aerospace Science and Technology (CASC200906).

**References**

[1] J.R. Miller, P. Simon, Electrochemical Capacitors for Energy Management, Science 321 (2008) 651－652.

[2] Y.M. Chiang , Building a Better Battery, Science 330 (2010) 1485－1486.

[3] C. Liu, F. Li, L.P. Ma, H.M. Cheng, Advanced materials for energy storage, Adv. Mater. 22 (2010) 28－62.

[4] D.A. Dikin, S. Stankovich, E.J. Zimney, R.D. Piner, G.H.B. Dommett, G.Evmenenko, S.T. Nguyen, R.S. Ruoff, Preparation and characterization of graphene oxide paper, Nature 448 (2007) 457－460.

[5] S. Park, K.S. Lee, G. Bozoklu, W. Cai, S.T. Nguyen, R.S. Ruoff, Graphene oxide papers modified by divalent ions-enhancing mechanical properties via chemical cross-linking, Acs Nano 2 (2008) 572－578.

[6] S. Stankovich, D.A. Dikin, G.H.B. Dommett, K.M. Kohlhaas, E.J.Zimney,E.A. Stach, R.D. Piner, S.T. Nguyen, R.S. Ruoff, Graphene-Based Composite Materials, Nature 442 (2006) 282 – 286.
[7] D.W. Wang , F. Li , J.P. Zhao , W.C. Ren , Z.G. Chen , J. Tan , Z.S. Wu ,I. Gentle , G.Q. Lu , H.M. Cheng , Fabrication of Graphene/Polyaniline Composite Paper via in Situ Anodic Electropolymerization for High-Performance Flexible Electrode, Acs Nano 3 (2009) 1745 – 1752.
[8] J.J. Wang , M.Y. Zhu , R.A. Outlaw , X. Zhao , D.M. Manos ,B.C. Holloway , Synthesis of carbon nanosheets by inductively coupled radio-frequency plasma enhanced chemical vapor deposition, Carbon 42 (2004) 2867 – 2872.
[9] J.S. Bunch, A.M. Van Der Zande, S.S. Verbridge, I.W. Frank, D.M. Tanenbaum, J.M. Parpia, H.G. Craighead, P.L. McEuen, Electromechanical Resonators from Graphene Sheets, Science 315 (2007) 490 – 493.
[10] K.S. Novoselov, A.K. Geim, S.V. Morozov, D. Jiang, Y. Zhang, S.V.Dubonos, I.V.Grigorieva, A.A. Firsov, Electric Field Effect in Atomically Thin Carbon Films, Science 306 (2004) 666 – 669.
[11] S. Stankovich, D.A. Dikin, R.D. Piner, K.A. Kohlhaas, A. Kleinhammes, Y. Jia, Y. Wu, S.T. Nguyen, R.S. Ruoff, Synthesis of graphene-based nanosheets via chemical reduction of exfoliated graphite oxide, Carbon 45 (2007) 1558 – 1565.
[12] X.B. Fan, W.C. Peng, Y.Li, X.Y. Li, S.L. Wang, G.L. Zhang, F.B.Zhang, Deoxygenation of exfoliated graphite oxide under alkaline conditions: a green route to graphene preparation, Adv. Mater. 20 (2008) 4490 – 4493.
[13] Z. Yu, B. Duong, D. Abbitt, J. Thomas, Highly ordered $MnO_2$ nanopillars for enhanced supercapacitor performance, Adv. Mater. 25 (2013) 3302 – 3306.
[14] M. Huang, Y. Zhang, F.Li, L. Zhang, R.S. Ruoff, Z. Wen, Q. Liu, Self-assembly of mesoporous nanotubes assembled from interwoven ultrathin birnessite-type $MnO_2$ nanosheets for asymmetric supercapacitors, Sci. Rep. 4 (2014) 3878.
[15] W.B. Choi, I.D. Lahiri, R.H. Seelaboyina, Synthesis of Graphene and Its Applications: A Review, Solid State and Materials Sciences 35 (2010) 52 – 71.
[16] J.Yan, J.F. Zhang, W. Tong, Fast and reversible surface redox reaction of graphene -$MnO_2$ composites as supercapacitor electrodes, Carbon 48 (2010) 3825 – 3833.
[17] S. Chen, J. Zhu, X. Wu, Q. Han, X. Wang, Graphene oxide--$MnO_2$ nanocomposites for supercapacitors, ACS Nano 4 (2010) 2822 – 2830.
[18] Z.S. Wu, W. Ren, D.W. Wang, F. Li, B. Liu, H.M. Cheng, High-energy $MnO_2$ nanowire/graphene and graphene asymmetric electrochemical capacitors, ACS Nano 4 (2010) 5835 – 5842.
[19] Y. Xu, K. Sheng, C. Li, G. Shi, Self-Assembled Graphene Hydrogel via a One-Step Hydrothermal Process, ACS Nano 4 (2010) 4324 – 4330.
[20] B.G. Choi, M. Yang, W.H. Hong, J.W. Choi, Y.S. Huh, 3D macroporous graphene frameworks for supercapacitors with high energy and power densities, ACS Nano 6 (2012) 4020 – 4028.
[21] K.W. Nam, K.B. Kim, A study of the preparation of NiOx electrode via electrochemical route for supercapacitor applications and their charge storage mechanism, J. Electrochem. Soc. 149 (2002) A346 – A354.

[22] L. Zhang, X.S. Zhao, Carbon-based materials as supercapacitor electrodes, Chem Soc Rev. 38 (2009) 2520–2531.
[23] S.B. Ma, K.Y. Ahn , E.S. Lee, K.H. Oh, K.B. Kim, Synthesis and characterization of manganese dioxide spontaneously coated on carbon nanotubes, Carbon 45 (2007) 375–382.
[24] A. Ogata, S. Komaba, R. Baddour-Hadjean, J.P. Pereira-Ramos, N. Kumagai, Doping effects on structure and electrode performance of K-birnessite-type manganese dioxides for rechargeable lithium battery, Electrochim. Acta 53 (2008) 3084–3093.
[25] J.F. Zhuang, J. Yan, W. Tong , L.J. Zhi, G.Q. Ning, T.Y. Li, F. Wei, Asymmetric Supercapacitors Based on Graphene/$MnO_2$ and Activated Carbon Nanofiber Electrodes with High Power and Energy Density, Adv. Funct.Mater. 21 (2011) 2366–2375.
[26] M. Nakayama, T. Kanaya, R. Inoue, Anodic deposition of layered manganese oxide into a colloidal crystal template for electrochemical supercapacitor, Electrochem. Commun. 9 (2007) 1154–1158
[27] M. Nakayama, T. Kanaya, J.W. Lee, B.N. Popov, Electrochemical synthesis of birnessite-type layered manganese oxides for rechargeable lithium batteries, J. Power Sources 179 (2008) 361–366.
[28] Z. Weng, Y. Su, D.W. Wang, F. Li, J. Du, H.M. Cheng, Graphene-cellulosepaper flexible supercapacitors, Adv. Energy Mater. 1 (2011) 917–922.
[29] A. Ramadoss, S.J .Kim, Improved activity of a graphene–$TiO_2$ hybrid electrode in an electrochemical supercapacitor, Carbon 6 3 ( 2 0 1 3 ) 4 3 4 – 4 4 5
[30] A. Burke, R&D considerations for the performance and application of electrochemical capacitors, Electrochim. Acta 53 (2007) 1083–1091.
[31] S.J .He, W .Chen, High performance supercapacitors based on three-dimensional ultralight flexible manganese oxide nanosheets/carbon foam composites, J. Power Sources 262 (2014) 391–400.
[32] B.G .Choi, M.H .Yang, W.H .Hong, J.W .Choi, Y.S .Huh, 3D Macroporous Graphene Frameworks for Supercapacitors with High Energy and Power Densities, ACS Nano 6 (2012) 4020–4028.
[33] Y.W. Cheng, S. Lu, H. Zhang, C.V. Varanasi, J. Liu, Synergistic Effects from Graphene and Carbon Nanotubes Enable Flexible and Robust Electrodes for High-Performance Supercapacitors, Nano Lett. 12 (2012) 4206–4211.
[34] V. Khomenko, E. Raymundo-Pinero, E. Frackowiak, F. Beguin, High-voltage asymmetric supercapacitors operating in aqueous electrolyte, Appl. Phys. A Mater. Sci. 82 (2006) 567–573.
[35] L.F. Chen, Z.H. Huang, H.W. Liang, Q.F.Guan, S.H. Yu, Bacterial-cellulose-derived carbon nanofiber@MnO2 and nitrogen-doped carbon nanofiber electrode materials: An asymmetric supercapacitor with high energy and power density, Adv. Mater. 25 (2013) 4746–4752.
[36] M.S. Hong, S.H. Lee, S.W. Kim, Use of KCl Aqueous Electrolyte for 2 V Manganese Oxide/Activated Carbon Hybrid Capacitor, Electrochem. Solid-State Lett. 5 (2002) 227–230.

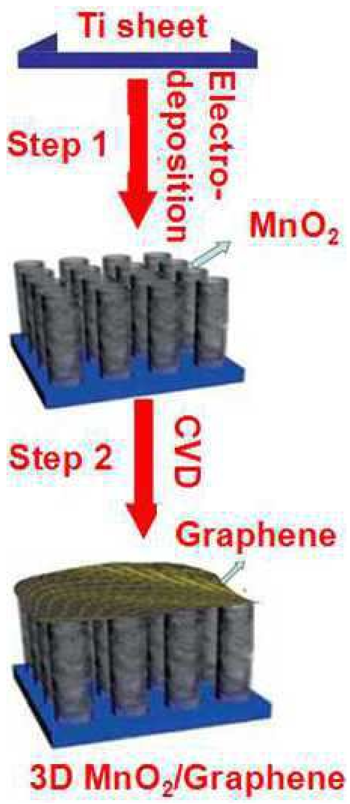


**Scheme 1.** Synthetic scheme of the 3D $MnO_2$/GR composite.

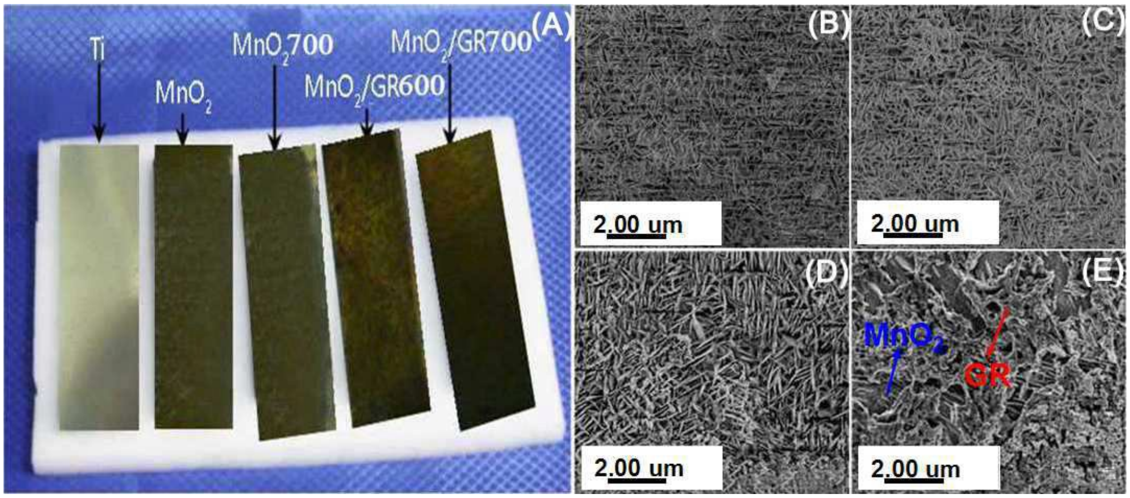


**Fig. 1.** (A) Photographs of Ti, $MnO_2$, $MnO_2$700 ($MnO_2$ heated in 700 $^oC$), and $MnO_2$/GR composites at different temperature. (B,C) SEM images of $MnO_2$ before and after the heating. (D,E) SEM images of 3D $MnO_2$/GR in 600 and 700 $^oC$, respectively.

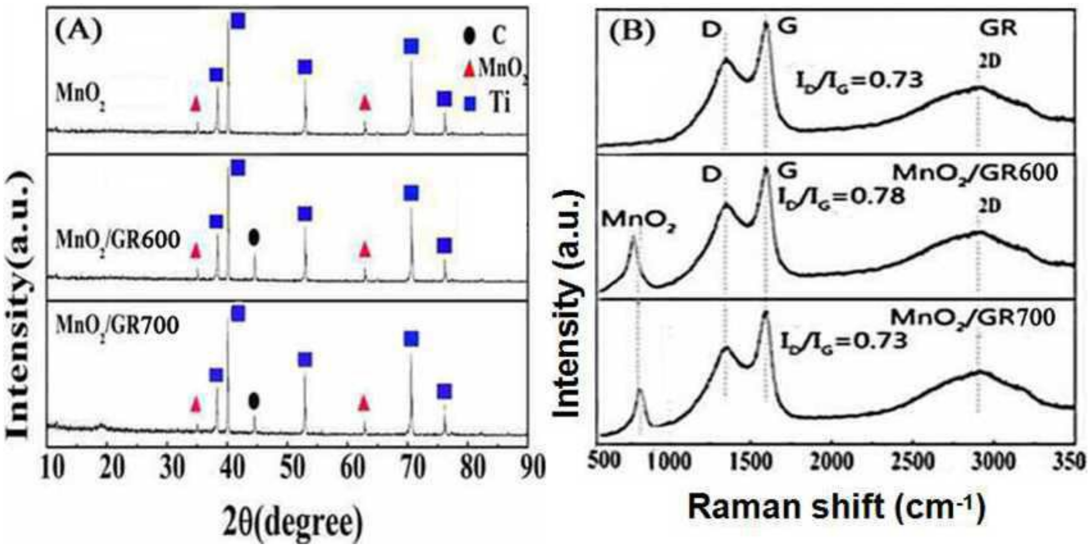


**Fig. 2.** (A) XRD patterns of the $MnO_2$ nanowall electrodeposited and the GR grown on the surface of the $MnO_2$ nanowall substrates at 600 and 700 °C, respectively. (B) Raman spectra of pure GR (700 °C) after the $MnO_2$ nanowall was removed and the GR grown on the surface of the $MnO_2$ nanowall substrates at 600 and 700 °C, respectively.

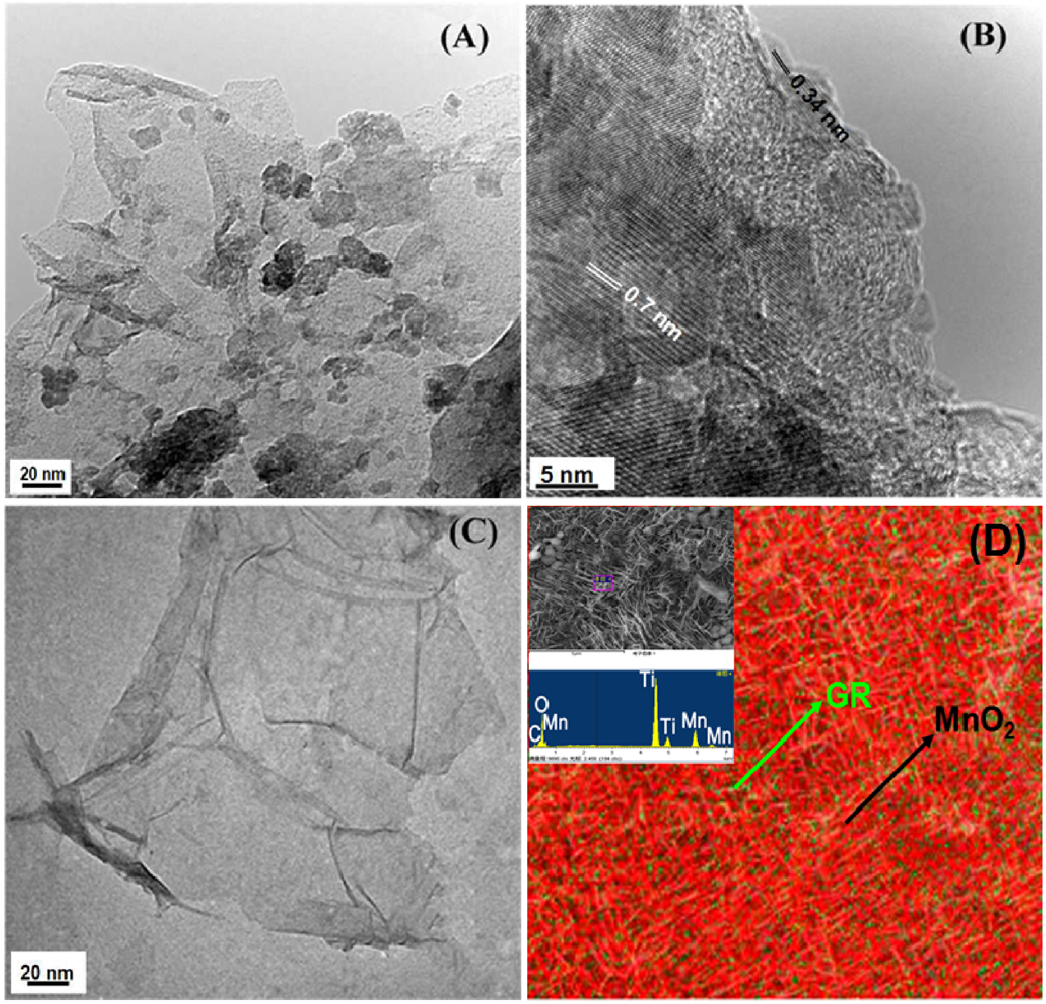


**Fig. 3.** (A) Low and (B) high magnification TEM images of $MnO_2$/GR700 composite, showing the graphene covered on the surface of the $MnO_2$ nanowall. (C) The TEM images of pure graphene after the $MnO_2$ nanowall was removed. (D) The scanning electron microscopic elemental map of 3D $MnO_2$/GR composite.

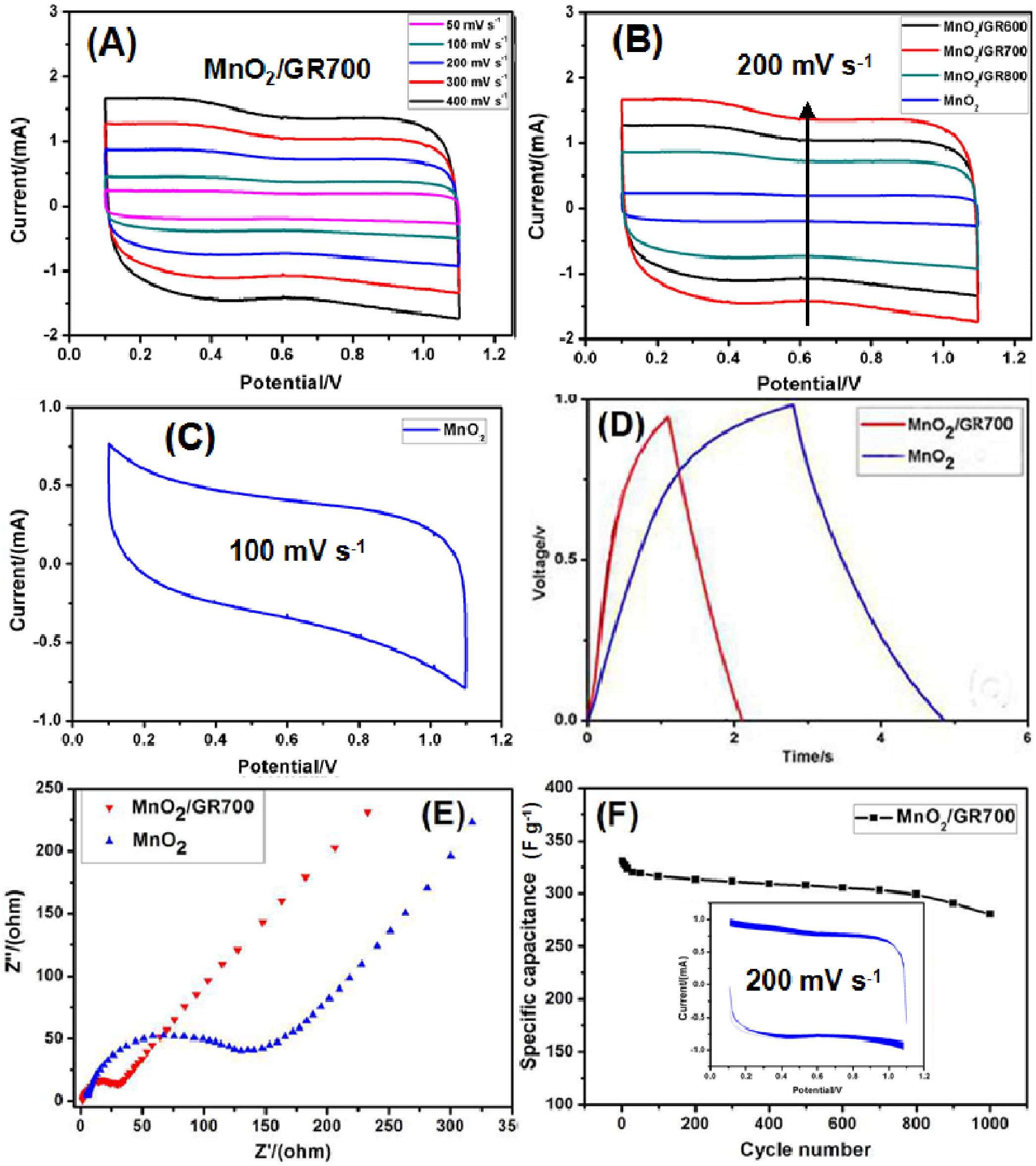


**Fig. 4.** (A) CV curves of the $MnO_2$/GR700 composite at different scan rates. (B) Comparison CV curves of the $MnO_2$/GR600, $MnO_2$/GR700, $MnO_2$/GR800 and $MnO_2$ at the scan rate of 200 mV $s^{-1}$. (C) CV curves of $MnO_2$ with absence of GR at the scan rate of 100 mV $s^{-1}$. (D) Galvanostatic charge-discharge of the $MnO_2$/GR700 and $MnO_2$. (E) Ragone and Nyquist plots of the supercapacitors based on the $MnO_2$/GR700 and $MnO_2$. (F) Cycle life curves of the supercapacitors based on $MnO_2$/GR700 composites at the scan rate of 200 mV $s^{-1}$.

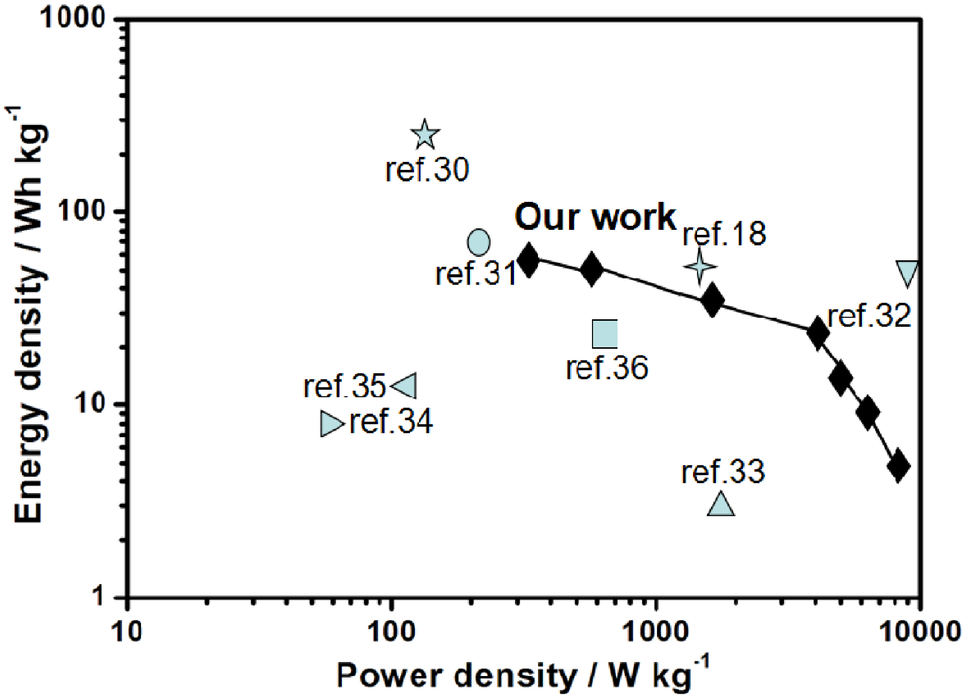


Fig. 5 Ragone plot of the energy density vs. power density for batteries and carbon-based supercapacitors.

## Graphical abstract